Journal of The Electrochemical Society, **146** (4) 1279-1289 (1999)
S0013-4651(98)05-018-6 CCC: $7.00 © The Electrochemical Society, Inc.

Solid-State Electrochemical Kinetics of Li-Ion Intercalation into $Li_{1-x}CoO_2$: Simultaneous Application of Electroanalytical Techniques SSCV, PITT, and EIS

M. D. Levi,[a,*] G. Salitra,[a] B. Markovsky,[a] H. Teller,[a] D. Aurbach,[a,*] Udo Heider,[b] and Lilia Heider[b]

[a]*Department of Chemistry, Bar-Ilan University, 52900 Ramat-Gan, Israel*
[b]*Merck KGaA, 64293 Darmstadt, Germany*

The electroanalytical behavior of thin $Li_{1-x}CoO_2$ electrodes is elucidated by the simultaneous application of three electroanalytical techniques: slow-scan-rate cyclic voltammetry (SSCV), potentiostatic intermittent titration technique, and electrochemical impedance spectroscopy. The data were treated within the framework of a simple model expressed by a Frumkin-type sorption isotherm. The experimental SSCV curves were well described by an equation combining such an isotherm with the Butler-Volmer equation for slow interfacial Li-ion transfer. The apparent attraction constant was -4.2, which is characteristic of a quasi-equilibrium, first-order phase transition. Impedance spectra reflected a process with the following steps: Li^+ ion migration in solution, Li^+ ion migration through surface films, strongly potential-dependent charge-transfer resistance, solid-state Li^+ diffusion, and accumulation of the intercalants into the host materials. An excellent fit was found between these spectra and an equivalent circuit, including a Voigt-type analog (Li^+ migration through multilayer surface films and charge transfer) in series with a finite-length Warburg-type element (Li^+ solid-state diffusion), and a capacitor (Li accumulation). In this paper, we compare the solid-state diffusion time constants and the differential intercalation capacities obtained by the three electroanalytical techniques.

Manuscript submitted May 8, 1998; revised manuscript received November 5, 1998.

$Li_{1-x}CoO_2$ is an important cathode material for high-energy-density, rechargeable Li-ion batteries.[1-13] Li intercalation into this compound occurs via several phase transition processes.[1,12] The most distinctive process appears as a pair of sharp reversible peaks in the cyclic voltammetry of these electrodes at a sufficiently slow scan. This process occurs in the $0 < x < 0.25$ range (3.6-4.0 V vs. Li/Li^+) and corresponds to a first-order transition between two different hexagonal phases.[1,12]

The present paper deals with the electroanalytical response of $Li_{1-x}CoO_2$ electrodes in the given range of x obtained by simultaneous application of slow-scan-rate cyclic voltammetry (SSCV), potentiostatic intermittent titration (PITT), and electrochemical impedance spectroscopy (EIS).[14-17]

We previously applied a similar approach for the study of lithiated graphite electrodes,[14-17] which revealed that the electroanalytical behavior of these electrodes may be well understood in terms of the existence of strong attractive interactions between intercalation sites.[18] This paper aims at extending such an approach to $Li_{1-x}CoO_2$ electrodes ($0 < x < 0.25$). Similar to lithiated graphite, $Li_{1-x}CoO_2$ is also a layered material.[1,12] Furthermore, our recent studies of several cathode materials.[19] showed that surface films, through which Li^+ ions migrate from solution phase to active mass, cover the $Li_{1-x}CoO_2$, as is the case with Li_xC_6. Consequently, similar electrochemical models may fit both Li_xC_6 and $Li_{1-x}CoO_2$ electrodes. The present paper provides a basis for the calculation of several important kinetic parameters related to intercalation reactions. Direct comparison among the various electrochemical techniques used is also presented and discussed in terms of applicability and accuracy.

Experimental

$LiCoO_2$ powder was obtained from Merck [2-3 μm particle size, 0.75 m^2/g specific surface area as determined by the Brunauer-Emmett-Teller (BET) method, using the Gemini 2375 system from Micromeritics, Incorporated]. The electrode's active mass was 85 wt % $LiCoO_2$, 10 wt % conductive carbon black, and 5 wt % polyvinylidene fluoride (PVDF) binder. These substances were thoroughly mixed with an appropriate amount of 1-methyl-2-pyrrolidone, with subsequent sonication in a test tube. Using a micropipette, several drops of this suspension (under continuous sonication) were removed from the middle level of the tube, then uniformly spread on one side of a heated 1.2 × 1.2 cm piece of Al foil. After drying in an oven at 150°C, the other side of the foil was similarly covered with the same active mass. Each electrode contained about 1 mg of the active mass (a few microns thick).

We also performed ex situ X-ray diffraction (XRD) measurements of differently oriented $Li_{1-x}CoO_2$ electrodes. In brief, the XRD patterns and the evaluated lattice parameters of $LiCoO_2$ from Merck revealed almost identical properties to those reported by both Ohzuku and Ueda,[12] and Reimers and Dahn.[1]

The three-electrode cell and solutions were the same as those used in our studies of Li-ion intercalation into graphite.[14-17] It contains a polyethylene frame with symmetrical slits on both sides holding the working and counter electrodes in a parallel-plate configuration with Li counter and reference electrodes.

The electrolyte solution was 1 M $LiAsF_6$ (Lithco) in an ethylene carbonate (EC)-dimethyl carbonate (DMC) 1:3 mixture (Merck's solvents). All other details, including glove-box operation and electrochemical measurements, were reported in previous publications.[20,21]

In brief, EIS was applied using Schlumberger's 1286 electrochemical interface and 1255 frequency response analyzer driven by the Corrware software from Scribner Associates (486 IBM PC). PITT and differential capacity vs. electrode potential curves (the latter being similar to the cyclic voltammetric curves at different scan rates) were performed using a multichannel Arbin system driven by a Pentium IBM PC.

Our approach to the performance of PITT measurements and their interpretation in terms of the finite-space diffusion models already has been reported.[15] In this work, 10 mV height steps were applied in the vicinity of the differential capacity peak, 3.93–3.96 V, 20 mV height in the range of 3.85–3.93 and 3.96–3.98 V, and 50 mV height in the 3.98–4.33 V range. Each subsequent step was applied after an equilibration was reached during the preceding step. The residual (background) currents were less than 0.2 μA/mg (of the active mass) in the range of 3.85–4.10 V and increases to 0.4–0.5 μA/mg in the 4.10–4.35 V range (equilibration time in all cases did not exceed 5 h). The key point in obtaining accurate values of the diffusion coefficient, within a range of potentials far from the differential capacity peak, is the application of a sufficiently high potential step so that the amount of charge injected into the electrode during the step is always considerably higher than the parasitic charge related to the residual current.[15]

---

* Electrochemical Society Active Member.

S0013-4651(98)05-018-6 CCC: $7.00

Theory

Kinetic model for the voltammetric behavior of $Li_{1-x}CoO_2$.—We assume that the use of thin $Li_{1-x}CoO_2$ electrodes enables us to eliminate some of the complications due to ohmic potential drop and Li diffusion in porous electrodes. Hence, we attribute the electroanalytical response of these electrodes to the accumulation (sorption) of lithium in the single particles (which is potential-dependent), complicated by slow ion migration, charge transfer, and solid-state diffusion. Our recent studies of lithiated graphite electrodes and related modeling demonstrated a similarity between intercalation and adsorption processes in terms of their electroanalytical response.[14-17]

Consequently, the intercalation process of lithium into thin $Li_{1-x}CoO_2$ electrodes can be described and treated similarly as adsorption processes at the metal/solution interface,[22-25] and the charging (doping) of conventional redox and electronically conducting polymers.[26-28] Recently, Conway[25] provided evidence for the close similarity between the adsorption (UPD) and intercalation processes arising from fundamental thermodynamic reasons. A basic characteristic describing an intercalation process is its sorption isotherm.[25] The SSCV of $Li_{1-x}CoO_2$ in the $0 < x < 0.25$ (3.6–4.0 V vs. Li/Li^+) range has a major relatively narrow redox peak. Following the results of Ref. 25, such a sorption process can be treated by a Frumkin-type sorption isotherm, accounting for possible interactions between the intercalated species, which has the classical form

$$x/(1 - x) = \exp[f(E - E_o)] \exp(-gx) \qquad [1]$$

E and E_o define the electrode's real and standard potentials in the equilibrium state, x is the intercalation level (i.e., the mole fraction of the species), and g reflects the interaction between the intercalation sites in $Li_{1-x}CoO_2$ (positive for repulsion and negative for attraction); $f = F/RT$ (F is the Faraday constant, R is the gas constant, and T is absolute temperature. However, practical intercalation processes can hardly proceed at ideal equilibrium conditions and are always complicated by kinetic limitations, such as slow interfacial charge transfer. It should be noted that a similar approach for describing the energetics of Li insertion into $Li_{1-x}CoO_2$ also appears in a recent publication by Ohzuku et al.[4]

The following simplified approach was adopted. The sorption isotherm 1 was combined with a Butler-Volmer equation, which accounts, in this case, for the slow Li-ion interfacial charge transfer. Note that the combined equation has a form similar to that previously used for the analysis of differential capacity curves obtained during redox reactions of adsorbed species,[29,30] electroactive polymers,[27,28,31] and Li-ion intercalation into graphite[14,16]

$$I = (k_o/\delta f\nu)\{(1 - x)\exp[-(1 - \alpha)gx]\exp[(1 - \alpha)f(E - E_o)] - x\exp(\alpha gx)\exp[-\alpha f(E - E_o)]\} \qquad [2]$$

Here I is the dimensionless current and $K = (k_o/\delta f\nu)$ is the dimensionless rate constant, with k_o representing the standard heterogeneous rate constant (cm/s) and ν the potential scan rate; δ is a characteristic size of the active mass (the depth of the electrochemical reaction). The charge-transfer coefficient, α, in Eq. 2 was assumed to be symmetrical for the anodic and cathodic branches. An accurate initial approximation for many electrochemical reactions is $\alpha = 0.5$. The number of Li ions per unit intercalation site was assumed to be one, corresponding to the following stoichiometry

$$4LiCoO_2 \rightleftarrows 4Li_{0.75}CoO_2 + e^- + Li^+ \qquad [3]$$

This stoichiometry relates exactly to the two-phase region at $0 < x < 0.25$, for $Li_{1-x}CoO_2$ (3.6–4.0 V vs. Li/Li^+), as evidenced from in situ XRD measurements.[1,12] Beyond kinetic control (i.e., at sufficiently large k_o or low δ and ν), the behavior should approximate equilibrium (quasi-equilibrium) behavior, and thus Eq. 2 is reduced to the Frumkin isotherm, Eq. 1, whereas the equilibrium differential capacity curves ($C_{int}(E) = [I(E)/\nu]$ are conveniently represented in the following dimensionless form[27]

$$C_{int}\ (\text{dimensionless}) = [g + 1/x + 1/(1 - x)]^{-1} \qquad [4]$$

Simulation of the C_{int} vs. E-plots through Eq. 4 and 1 is straightforward and easily performed. Theoretical cyclic voltammetry (CV) curves were calculated according to Eq. 2 using potential steps of 0.001 V. Each additional step required numeric integration of the current calculated for the preceding one (potential limits are given in V) in order to find the proper $x(E)$, which is incorporated in Eq. 2

$$x(E) = f\int_{-0.3}^{0.3} I(E - E_o)\,dE \qquad [5]$$

The computation was performed using Microsoft Excel for Windows 95. Note that $x = 0$ in Eq. 1-5 corresponds to $Li_{0.75}CoO_2$.

Equations 1-5 ignore possible complications by the slow, solid-state diffusion step. This may be justified for thin electrodes and sufficiently slow scan rates. At high scan rates, the CV behavior may be dominated by the solid-state Li-ion diffusion within the particle's bulk (finite-space diffusion-controlled CV). In such a case, the following equation derived in Ref. 32 is formulated

$$I_p = 0.446\,nFA\,(D/\delta)\,c_R\beta^{0.5}\tanh(0.56\beta^{0.5} + 0.05\beta) \qquad [6]$$

where I_p (amperes) is the peak current; A (cm^2) is the electrode surface area; D (cm^2/s) denotes the chemical diffusion coefficient of the reactive species, c_R (mol/cm^3) is their bulk concentration; δ (cm) is the electrode thickness; and $\beta = nf\nu\,(\delta^2/D)$ (a dimensionless characteristic time parameter).

At relatively high scan rates ($\delta^2/D >> 1/f\nu$, $\beta >> 1$), Eq. 6 assumes the classical Randles-Sevchik equation for semi-infinite diffusion[32]

$$I_p = 0.446\,n^{1/2}FAf^{1/2}D^{1/2}\nu^{1/2}c_R \qquad [7]$$

In the Randles-Sevchik equation (Eq. 7) for solution redox species, c_R is independent of the electrode potential. However, in the present case (finite-space diffusion), c_R corresponds to a concentration of Li in the active mass and is strongly potential dependent, according to a sorption isotherm.

Our treatment of the kinetic effects in the voltammetry of intercalation systems is an alternative to that previously proposed by Dahn and Haering[33] who used a large constant ohmic impedance in series with the intercalation process with *completely flat* charge and discharge curves. They also included solid-state ion diffusion via movement of the distinct interfacial boundary in the electrode bulk. Note that in all cases, the model proposed in Ref. 33 predicts a linear I_p vs. $\nu^{1/2}$ plot, which is in contrast to our experimental data that show a linear dependence of I_p vs. ν for relatively small scan rates.

Kinetic models for the EIS and PITT responses of thin $Li_{1-x}CoO_2$ electrodes and their link to the CV model.—The similarity between Li intercalation processes into graphite and $Li_{1-x}CoO_2$ both include Li^+ migration through surface films,[19] interfacial charge-transfer, solid-state Li^+ diffusion, and accumulation (sorption) in the bulk via a phase transition. This similarity justifies the adoption of closely related impedance models for both electrodes. Thus, the equivalent circuit analog of Fig. 1 (see detailed discussion in Ref. 14) was also fitted to impedance spectra measured from $Li_{1-x}CoO_2$ electrodes.

From PITT, we calculate two important parameters. The first is the diffusion time $\tau = l^2/D$, where D is the chemical diffusion coefficient as previously defined and l is a characteristic diffusion length. The second parameter is the differential intercalation capacitance $C_{int} = Q_t\,(dx/dE)$. (Q_t is the overall intercalation charge for the processes studied.) Q_t and thus C_{int} are proportional to the electrode thickness, δ. For layered materials such as $Li_{1-x}CoO_2$ or Li_xC_6, the diffusion length l is not δ but rather a characteristic dimension of an average particle. We assume that Li-ion diffuse through a cross section perpendicular to the particle's basal planes, therefore, l is the average particle radius (or half the average particle size) which is 2-3 μm for our $Li_{1-x}CoO_2$ particles [from BET and scanning electron microscopy (SEM) analysis].

According to the PITT theory,[34,35] τ is related to the amount of the inserted (deinserted) charge during a small potential step, $\Delta Q = Q_t\Delta x$, by a simple formula

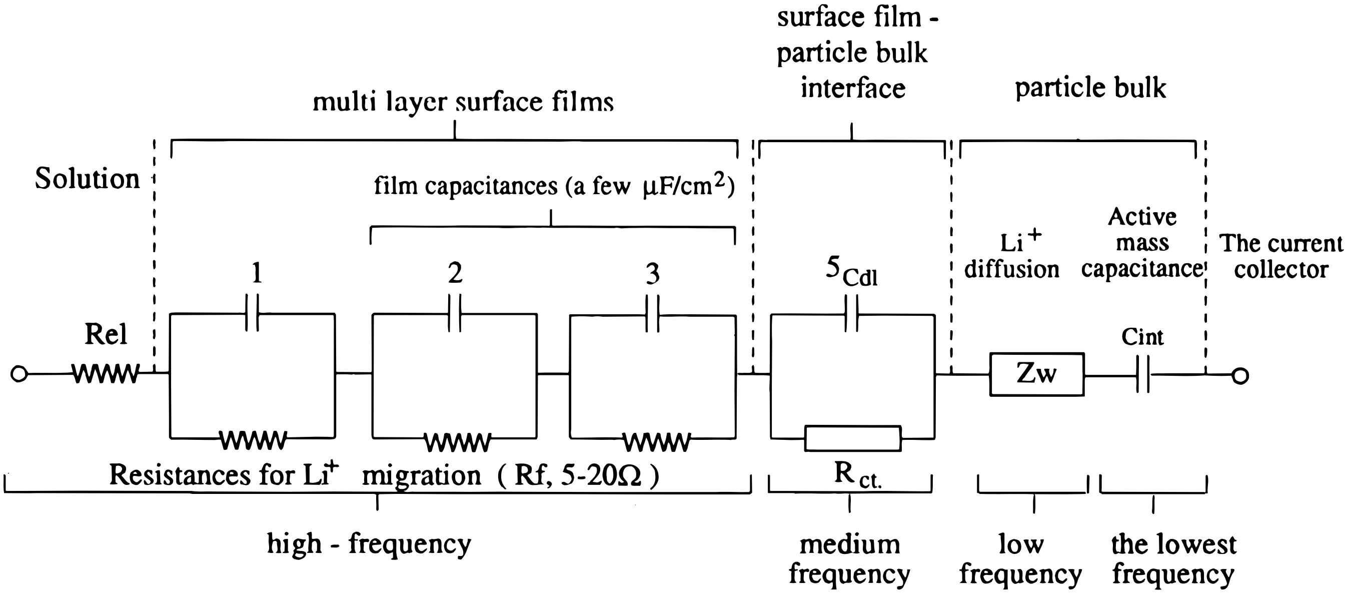

Figure 1. Equivalent circuit analog based on a combination of a Voigt-type analog and the generalized FMG impedance model. The various time constants to which the model refers are also presented.

$$\tau = [Q_t \Delta x/\pi^{1/2}\, It^{1/2}]^2 \text{ at } t << \tau \qquad [8]$$

Here, Q_t is the overall amount of charge (confined by the number of available intercalation sites), and $It^{1/2}$ is a Cottrell slope that is constant in the short time domain and is dependent on the electrode potential.[15] This equation is valid (τ independent of ΔE) only for sufficiently small potential steps.

Regarding EIS, the time constant for the finite-space solid-state diffusion depends on the Warburg slope, $A_w = \Delta\mathrm{Re}/\Delta\omega^{-1/2} = \Delta\mathrm{Im}/\Delta\omega^{-1/2}$ (ΔRe and ΔIm are the differences between the real and imaginary components of the impedance, corresponding to a finite variation in the frequency $\Delta\omega$), and the differential capacity $Q_t dx/dE$ [36]

$$\tau = 2[Q_t A_w dx/dE]^2 \qquad [9]$$

Properly designed PITT and EIS experiments should lead to the same values of τ and hence, D.

We can calculate the diffusion time, τ, from SSCV at sufficiently high scan rates via Eq. 7. Approximating the cross-sectional area for the diffusion process as A, and the diffusion length as l, $FAc_R = Q_t/l$, the diffusion time, τ, calculated from SSCV is

$$\tau = 0.199\, fn^3 (Q_t/I_p \nu^{-1/2})^2 \qquad [10]$$

$I_p\nu^{-1/2}$ is a characteristic SSCV parameter, independent of ν. However, SSCV clearly probes the average value of τ in the entire intercalation range, as is expected for a relaxation technique with a relatively high amplitude. In contrast, low-amplitude voltage steps in PITT and small amplitudes of the alternative current in EIS should normally result in τ, which is highly resolved with respect to the electrode potential.

The last quantity to be introduced is the differential intercalation capacity which relates to the low frequency (prolonged relaxation time) calculated from the three techniques as follows

$$\begin{aligned} C_{\mathrm{int}} &= I(E)/\nu && \text{(SSCV)} \\ C_{\mathrm{int}} &= Q_t \Delta x(E)/\Delta \mathrm{E} && \text{(PITT)} \qquad [11] \\ C_{\mathrm{int}} &= -\frac{1}{\omega Z''_{\omega\to 0}} && \text{(EIS)} \end{aligned}$$

$Z''_{\omega\to 0}$ is the imaginary part of the complex-plane impedance in the lowest frequency domain.

We analyze the consistency between the available SSCV and EIS data as follows: The charge-transfer resistance, R_{ct}, extracted from EIS (the diameter of the medium-frequency semicircle in the Nyquist plots as shown in the Results section), is connected with the heterogeneous rate constant, k_o, derived from the SSCV using Eq. 2. This connection is expressed by the following simplified equation

$$R_{ct} = \delta/[fQ_t k_o x^{0.5}(1 - x)^{0.5}] \qquad [12]$$

This equation implies the conventional definition of $R_{ct} = (nfi_o)^{-1}$ where i_o is the exchange current density. To derive i_o and hence Eq. 12, we followed the standard procedure described for solution redox couples.[37] We replaced the Nernst equation by the Frumkin isotherm (Eq. 1) with its further substitution into the second (cathodic) component of the net current (Eq. 2).

Equations1-12 provide a basis for the quantitative comparison between the kinetic and quasi-equilibrium characteristics of the Li intercalation processes of the $Li_{1-x}CoO_2$ electrode studied by simultaneous application of SSCV, PITT, and EIS.

Results

Cyclic voltammetry of the $Li_{1-x}CoO_2$ electrode.—Figure 2a shows a family of SSCV curves measured with an $Li_{1-x}CoO_2$ electrode in the range of ν from 500 to 10 μV/s. All the curves are normalized with respect to ν, and thus, they represent the differential capacity, C_{int}, of the electrode according to Eq. 11. At low scan rates, the height of I_p is approximately proportional to ν, whereas beyond some limit of higher scan rates, I_p becomes proportional to $\nu^{1/2}$. In addition, E_{pa}-E_{pc}, i.e., the difference between the corresponding anodic and cathodic peaks, and the half-peak width, $\Delta E_{p,1/2}$, gradually increase with ν. The anodic peak is higher (by a factor of 1.4) and narrower than the corresponding cathodic peak.

Figure 2b (the curve designated by open circles) shows a CV curve measured at the lowest scan rate that we applied, ν = 10 μV/s, at the condition most approaching equilibrium. The standard (formal) potential of reaction 1, approximated by a middle-peak potential, equals 3.903 V (vs. /Li$^+$), with the anodic peak E_{pa} = 3.933 V and the cathodic one E_{pc} = 3.872 V (see Fig. 2b). These three values are close to those obtained by Reimers and Dahn[1] from differential chronopotentiometry, 3.906, 3.923, and 3.888, respectively, and by Barker et al.[2] from differential capacity curves obtained using electrochemical voltage spectroscopy, 3.905, 3.940, and 3.870, respectively. These values, as well as those related to Ref. 1 (see the

S0013-4651(98)05-018-6 CCC: $7.00

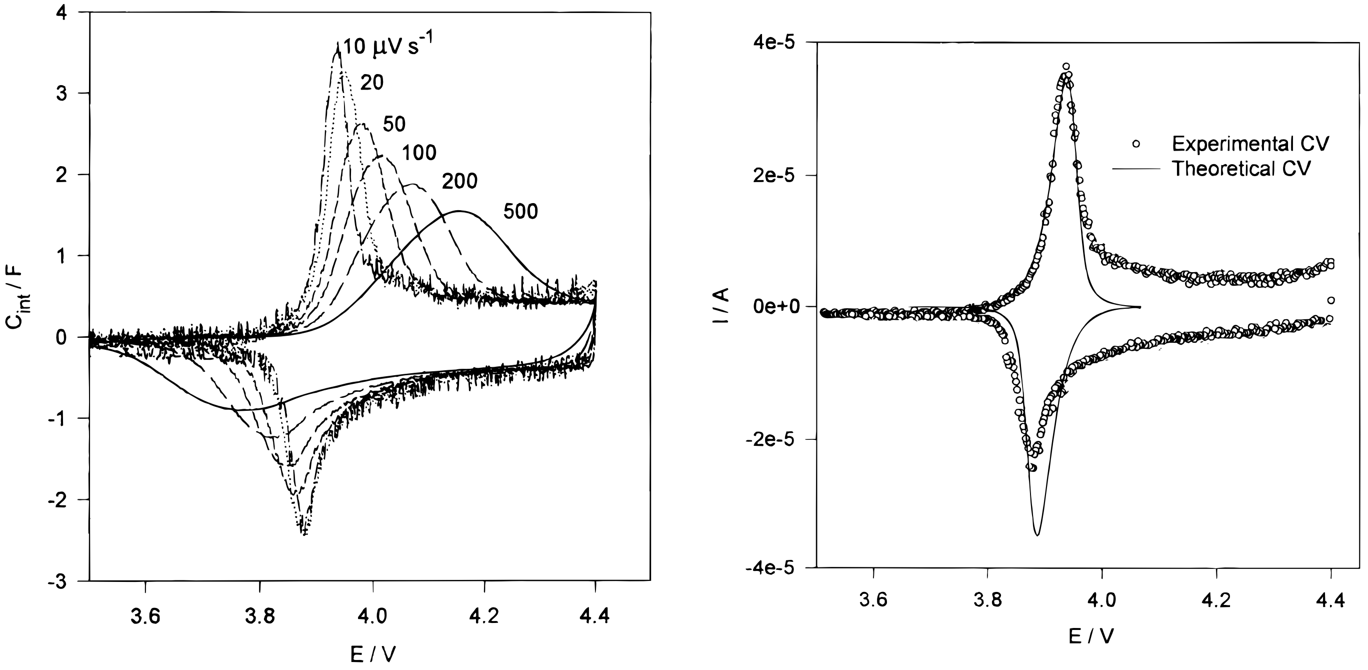

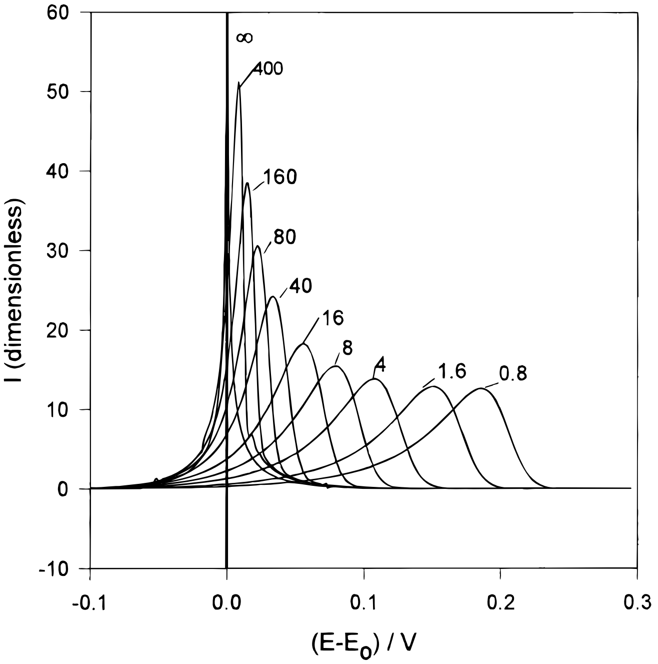

Figure 2. (a, above) Experimental plots of differential intercalation capacity. $C_{\mathrm{int}} = I/\nu$ vs. electrode potential measured at different scan rates as indicated in the figure. (b, top right) Comparison between the experimental CV curve ($\nu = 10$ μV/s) and that calculated according to Eq. 2 with $K = k_o/\delta f\nu = 40$ and $g = -4.2$. (c, right) A family of I vs. (E - E_o) curves calculated according to Eq. 2, using different values of the dimensionless constant rate K (as indicated in the figure) and $g = -4.2$.

following), were deduced from the figures appearing in the corresponding published papers and thus can be considered as rough estimations. The experiments described in Ref. 2 relate to an equivalent rate of C/100, whereas the equivalent rate of our SSCV measurements is about one order of magnitude higher.

However, the electrodes described in Ref. 2 were at least ten times thicker than ours (100 μm compared with <10 μm). In addition, the electrolyte system in Ref. 2 was polymeric, which may cause contact problems with part of the active mass. In the present case, the liquid electrolyte solution and the thin electrodes used ensure that all the active mass is in contact with the solution, and thus all the particles react simultaneously. Therefore, we assume that in most of the experiments described in this work, the electrodes are as close to equilibrium state as those in Ref. 2, in spite of the pronounced difference in the equivalent rate of the experiments, as mentioned previously. The middle-peak potential measured in the present study practically coincides also with the corresponding plateau on the plot of the open-circuit voltage vs. composition reported by Ohzuku and Ueda.[12] However, both the half-peak width and the peak-potential separation from the present work, 57 and 61 mV, respectively, are larger than the corresponding values obtained by Reimers and Dahn: $\Delta E_{\mathrm{pa},1/2} = 4\text{-}8$ mV, $\Delta E_{\mathrm{pc},1/2} = 32$ mV, and E_{pa}-$E_{\mathrm{pc}} = 35$ mV. [1] We ascribe this difference to the fact that the electrode used by Reimers and Dahn was closer to equilibrium charging conditions than that studied by us. This is supported by the following consideration. The differential chronopotentiogram in Ref. 1 was measured at a 50 h rate, which corresponds to ~25 h charge along the major peak related to the two-phase coexistence region. The CV in the present work, measured at $\nu = 10$ μV/s, corresponds to a charge equal to $(\Delta E_{\mathrm{pa},1/2} I_{\mathrm{p}})/\nu$. Thus, if our electrode is charged with

S0013-4651(98)05-018-6 CCC: $7.00 © The Electrochemical Society, Inc.

a constant current, I_p, the process related to the two-phase coexistence region should require only 5700 s.

It is significant that the pronounced hysteresis (peak potential separation) does not disappear even at the limit of slow rates such as C/50. [1] This indicates that the hysteresis is intrinsic in its nature and cannot be simply ascribed to a kinetic limitation.

The potential range from 4.0 to 4.4 V is characterized by a response that seems to be essentially capacitive. Modeling of such a response was beyond the scope of the present work. On the contrary, using Eq. 2 we described current response in the two-phase region. The slowest SSCV (measured at $\nu = 10\ \mu V/s$) was fitted first, using various combinations of the two parameters, g ($-5 < g < -2$) and a dimensionless rate constant $K = k_o/\delta f\nu$ ($-0.4 < \log K < 2.6$). We found that the best fit was reached at $g = -4.2$ and $K = 40$. In Fig. 2b, the solid line representing the model curve was calculated with these parameters (corresponding to $\nu = 10\ \mu V/s$.) A good resemblance between the shape of both curves was observed only for the anodic peak. The height of the theoretical cathodic peak is somewhat larger than that of the experimental one, whereas the peak potential separation on the SSCV curve agrees satisfactorily with the calculated one. We assume that the poorer fit to the cathodic peak should be somehow connected with the capacitive-like response in the range of potentials from 4.0 to 4.4 V.

It was of interest to verify the applicability of Eq. 2 for fitting the SSCVs measured at different scan rates. For this we calculated a family of CVs using the same value $g = -4.2$ and varying K between 0.4 and 400 (see Fig. 2c). Qualitatively, these simulated curves reveal a similar trend in variation with ν (or K) as the experimental ones. The theoretical and the experimental curves are in broad agreement in the range of ν between 10 and 50 $\mu V/s$. As a trend, we note two limiting ranges of ν, covering $\nu > 50\ \mu V/s$ and possibly $\nu < 10\ \mu V/s$, in which the theoretical (based on the above-mentioned model) and the experimental curves are expected to vary considerably. An important observation is that at scan rates above a certain limit (e.g., $\nu > 0.02$ mV/s), the experimental CV currents are dependent on the scan rate (Fig. 2a), whereas the theoretical CV currents (Fig. 2c) are expected to be independent of the scan rate. In our opinion our results indicate that at sufficiently low scan rates, the electrode's behavior is indeed kinetically controlled, as predicted by the model proposed. However, at sufficiently high scan rates, solid-state diffusion becomes the rate-determining process. Considering another limit of the very low scan rates, one can see from Fig. 2c that the peak current increases enormously approaching the shape described by a delta function. Two alternative models may be suggested for understanding the shape of the differential capacity curves measured in the limit of very small ν. The first model relates to a delta-function behavior of a phase transition.[33] However, it should be noted that it is practically impossible to obtain the spike-like behavior of I vs. E (delta function), even in the absence of kinetic limitation, because the high ohmic potential drops should flatten the peak current. The second model implies a change in the rate-determining step from the kinetic to a droplet-like formation of a new phase in the bulk of the old one.[28] However, to determine which model is better requires the performance of SSCV measurements at scan rates of the order of $\mu V/s$, almost one order of magnitude lower compared with the lowest scan rate used in this work (which was beyond the scope of this study).

Note that the optimal value $g = -4.2$ (from the fitting procedure) is more negative than the critical one in the Frumkin sorption isotherm, $g_{crit} = -4$. [14,27,28] This result is consistent with that obtained by Ohzuku and Ueda[4] who treated the charging curve of $Li_{1-x}CoO_2$ electrode by a model similar to the Frumkin sorption isotherm. From their reported interaction energy we found $g = -4.8$, a value which is in close proximity to ours.

EIS characterization of the $Li_{1-x}CoO_2$ electrode.—Figure 3a presents a family of Nyquist plots measured in the range of potentials from 3.89 to 4.07 V [at open-circuit voltage (OCV) conditions] along the anodic branch of the SSCV curve (i.e., during deintercalation). Each Nyquist plot possesses a high-frequency depressed semicircle, which also appears in spectra measured with a freshly prepared electrode immersed in the electrolyte solution before deintercalation, and a medium-frequency semicircle. The second semicircle is nearly perfect (undepressed), and its diameter drastically decreases as the potential increases. These two semicircles clearly reflect well-separated, different time constants of the Li insertion process. Fourier transform infrared (FTIR) measurements of these electrodes revealed that they are covered mostly with Li_2CO_3 surface films, probably formed by the reaction between the lithiated oxide and the CO_2 in the air. In fact, the high-frequency, depressed semicircle in Fig. 3a is potential-independent and resembles similar impedance spectral features of lithium and lithiated graphite electrodes (the SEI model[14]). A rough calculation of the capacitance related to the high-frequency semicircle leads to values of the order of 10^{-6} F/cm^2, typical of the capacitance of surface films comprised of Li_2CO_3 on Li and Li-graphite electrodes.

We attribute the medium-frequency semicircle to charge-transfer resistance related to slow Li^+-ion interfacial transfer, coupled with a capacitance at the surface film/$Li_{1-x}CoO_2$ particle interface. This interpretation is supported by the fact that this semicircle is highly dependent on the potential and the capacitance involved is high (several mF/cm^2). This rather high capacitance can be ascribed to the high surface area through which charge transfer occurs. This high surface area can be attributed partially to the porous structure of the electrode and to a rough structure at the film-particle interface. However, this interpretation is not the only one possible to describe these complicated systems. Alternative models have been proposed by others, e.g., Goodenough et al.[3]

At lower frequencies, we observed a narrow Warburg region followed by a steep sloping line at the lowest frequencies. These low-frequency features are masked by the large, second (charge-transfer) semicircle discussed previously, as the potential is lower (and thus, R_{CT} is higher according to the given interpretation of this feature). The Warburg region is assigned, naturally, to solid-state diffusion of Li ions into the bulk cathode material, while the steep sloping line reflects capacitive behavior at the very low frequencies (5 mHz in this study for practical reasons). We attribute this capacitive behavior to accumulation of the intercalant (Li) into the bulk. Hence, the impedance spectra measured from $Li_{1-x}CoO_2$ reflect an overall serial Li-insertion process that includes several steps whose time constants are clearly distinguished by EIS. All these features of the impedance spectra may be modeled by a combination of a Voigt-type and the so-called generalized Frumkin and Melik-Gaykazyan (FMG) impedance analog (Fig. 1).[14] The latter consists of an in-series combination of differential intercalation capacitance C_{int} (Eq. 11), and the classical finite-length Warburg element, Z_w (Eq. 13)[38]

$$Z_w = R_D\,(j\omega l^2/D)^{-1/2}\tanh(j\omega l^2/D)^{1/2} \qquad [13]$$

R_D is the low-frequency limit of Z_w and $l^2/D = \tau$ is the characteristic solid-state diffusion time constant. It should be noted that formula 13 combines, as limiting cases, both the finite-length and semi-inite diffusion Warburg elements, depending on the range of frequencies considered. At higher frequencies, the finite-length Warburg approaches the classical semi-infinite Warburg element with its characteristic slope, A_w. [38] Thus, τ can be calculated either from Eq. 9 with use of A_w and the differential capacity $(Q_t dx)/dE$, or directly from Eq. 13.

Figure 3a shows a typical fit of the experimental Nyquist plots with the Voigt-Frumkin and Melik-Gaykazyan model (Fig. 1) obtained in the range of potentials close to the anodic SSCV peak of the $Li_{1-x}CoO_2$ electrode. Typical values of the parameters calculated through the simulation procedure are indicated in Fig. 3b, which shows a Nyquist plot obtained at $E = 4.07$ V, and the curve fitted according to the model in Fig. 1. Figure 3c shows typical Nyquist plots obtained at the beginning of the deintercalation process. It should be noted that due to the large scale of this figure, it is impossible to see the high-frequency features which reflect Li-ion migration through the surface films. At certain low potentials (<3.87 V), R_{CT}

S0013-4651(98)05-018-6 CCC: $7.00

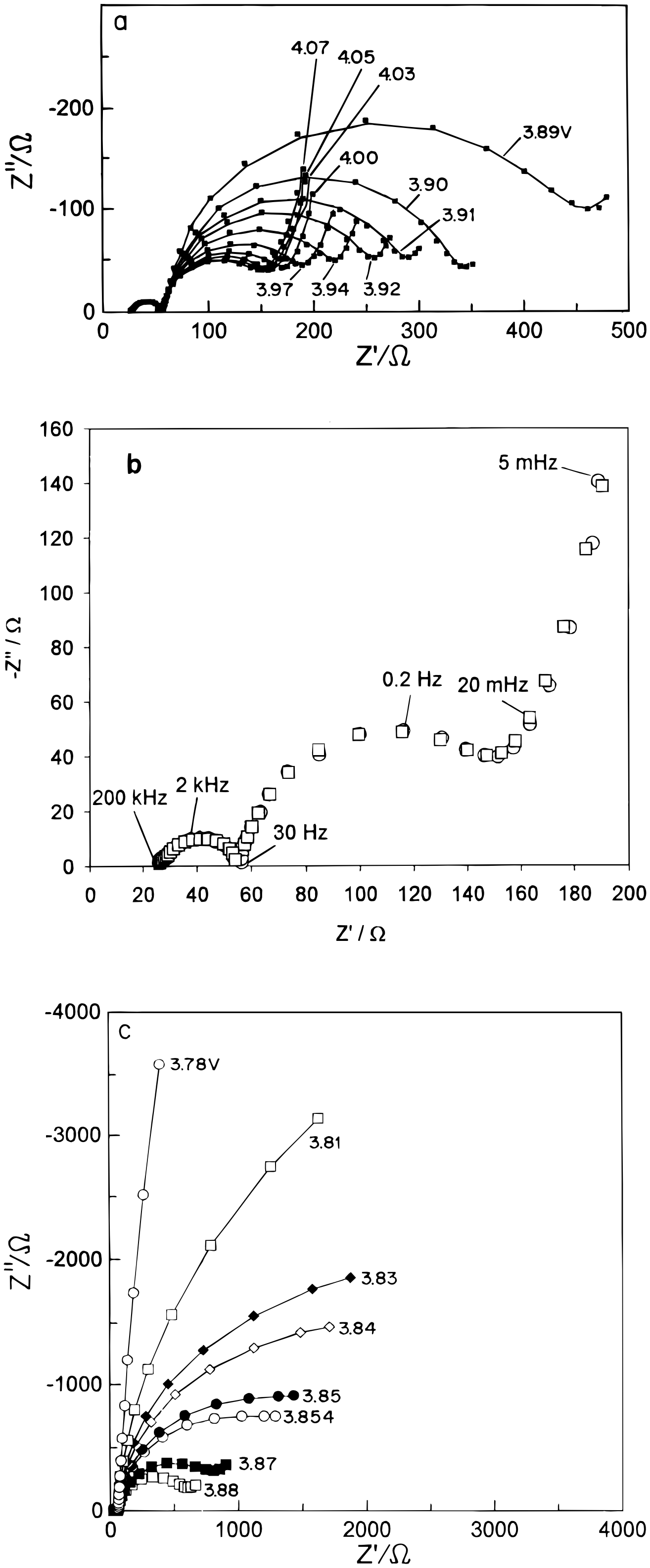

Figure 3. (a) Experimental Nyquist plots measured at different potentials (——), potential values indicated, and the simulated ones (■) for which the Voigt-FMG impedance model was used. (b) Experimental and simulated Nyquist plot of the $Li_{1-x}CoO_2$ electrode at $E = 4.07$ V shown in an enlarged scale. The following parameters were obtained by the simulation procedure: $C_{int} = 0.32$ F; $R_D = 161\ \Omega$, $\tau = l^2/D = 294$ s; the phase shift in the finite-length Warburg element was $\phi = 0.37$; $R_{CT} = 76\ \Omega$; $C_{DL} = 7.9$ mF; $R_1 = 13.7\ \Omega$; $C_1 = 1.24 \times 10^{-5}$ F; $R_2 = 3.23\ \Omega$; $C_2 = 9.9 \times 10^{-7}$ F; $R_3 = 11.5\ \Omega$; and $C_3 = 3.22 \times 10^{-6}$ F. (c) Experimental Nyquist plots obtained at the beginning of the deintercalation (the values of the potentials are indicated).

should be huge. Hence, the low-frequency curves shown in Fig. 3c probably reflect this huge R_{CT} (coupled with interfacial capacitance).

Figure 4a compares τ vs. E dependencies evaluated from the PITT and EIS (Eq. 8 and 9, respectively). Both graphs present narrow bell-shaped curves, with their maxima close to the voltammetric peak (SSCV), reaching $\tau \sim 1.1 \times 10^4$ s at the peak potential. Because the chemical diffusion coefficient is inversely proportional to τ ($D = l^2/\tau$), taking the value of $l = 2\ \mu$m from the BET and SEM studies, D can be presented as a function of E (Fig. 4b).

Figure 5 compares the dependencies of the charge-transfer resistance on the electrode potential obtained from the medium-frequency semicircle of the Nyquist plots and that calculated from the SSCV according to Eq. 12. We see that at the beginning of deintercalation (low potentials), R_{ct} obtained from the EIS is significantly higher than that obtained from the SSCV, whereas at higher potentials, the values of R_{ct} obtained from the two techniques are much closer to each other. We attribute the difference in the values of R_{CT} calculated from these two techniques to a certain limitation of SSCV as a large-amplitude technique.

Discussion

Comments on the simultaneous application of SSCV, PITT, and EIS techniques for studying the nature of intercalation reactions.—These three techniques have different resolution with respect to particular

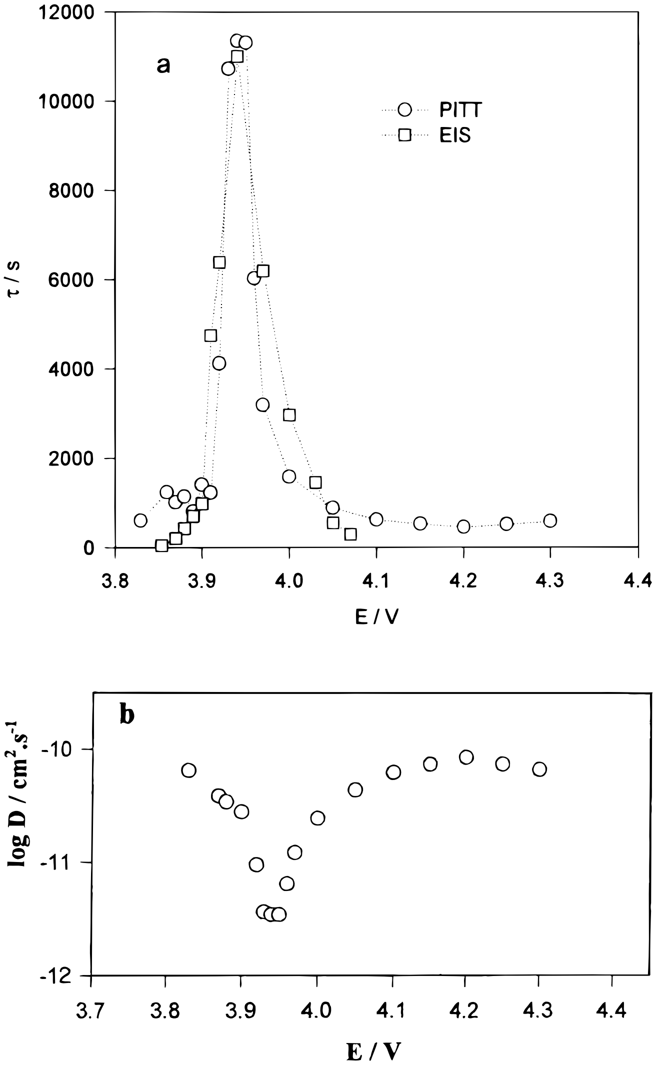

Figure 4. Plots of the characteristic diffusion time τ vs. E (a) and the chemical diffusion coefficient D vs. E (b) measured using PITT (a, b), Eq. 8, and EIS (a), Eq. 9.

S0013-4651(98)05-018-6 CCC: $7.00

rate-determining steps of different time constants, which contribute to the intercalation-deintercalation mechanism. For example, EIS is the most conclusive for studying Li-ion migration through the surface films (high-frequency domain), whereas PITT is more suitable for probing solid-state diffusion (the Cottrell domain). SSCV, which is a large-amplitude technique (compared with the other two), is suitable for probing the accumulation step (which involves phase transition) beyond diffusion control (low scan rates).

Several important characteristics of these electrodes can be calculated by two or all of these techniques, and such calculations provide a basis of comparison among them in terms of compatibility, accuracy, and resolution. These characteristics include the differential capacity, integral capacity, the diffusion coefficient, and the charge-transfer resistance. Figure 6 presents the peak-shaped features of C_{int} (differential capacity) obtained from SSCV, PITT, and EIS. The shift in the peak potential (within the range of 20 mV toward less positive values) in the previously described series of techniques certainly reflects deviation of the electrodes from equilibrium conditions during the measurements. The EIS spectra were measured at a number of different intercalation levels at OCV after prolonged potentiostatic equilibration. Thus, the results obtained from EIS reflect more of an equilibrium than the results obtained from the other two methods. The integral overall capacity of these electrodes is calculated from integration of the curves in Fig. 6. In Fig. 7 we present the results of this integration and the calculation for PITT and SSCV, which are similar for both techniques. We can explain the slight difference between the integral capacity calculated from PITT and SSCV at potentials above 4 V by the contribution of capacitive nonfaradaic currents that influence this technique's response.

Clearly from Fig. 6, the integral capacity obtained from EIS is considerably smaller than the capacity calculated by the other two techniques. (The C_{int} vs. E peak related to EIS in Fig. 6 is much narrower.) We attribute the low integral capacity calculated by the EIS to precision of the extrapolation of Z'' to $\omega \rightarrow 0$, required for calculating C_{int} (Eq. 11). In our measurements, however, the lowest frequency reached is only 5 mHz (due to practical reasons related to the experimental setup). Hence, to use EIS for precise quantitative measurements of C_{int} and the electrode's total charge capacity, the frequency limit applied should be lower than 5 mHz, and the intervals between the base potentials of the measurements should be the smallest possible.

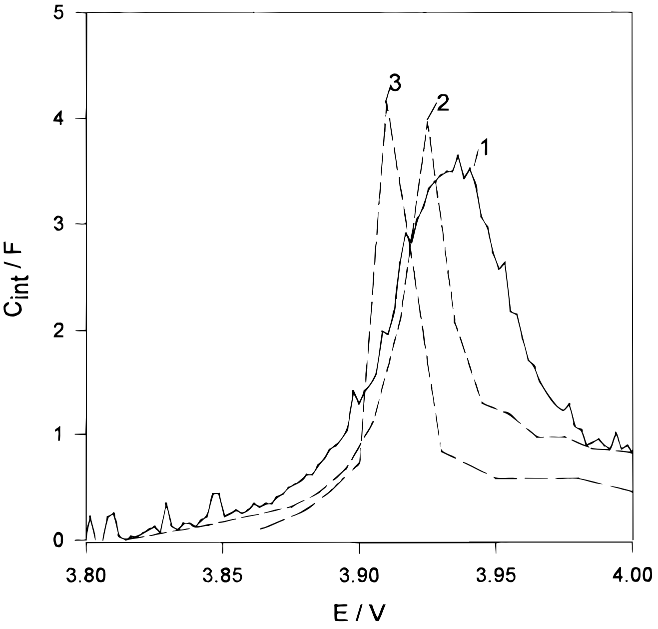

Figure 6. Plots of the intercalation capacity, C_{int}, vs. potential calculated from the experimental CV curve: (1) $C_{\text{int}} = I/\nu$, $\nu = 10$ μV/s; (2) PITT, $C_{\text{int}} = Q_t \Delta x(E)/\Delta E$; (3) the FMG impedance model, $C_{\text{int}} = -(1/\omega Z''_{\omega \rightarrow 0})$.

An important aspect of the simultaneous application of SSCV, PITT, and EIS is the comparison of the Li^+ chemical diffusion coefficient, D, calculated from the three methods.

SSCV possesses high resolution (in terms of the relation between the differential capacity and potential) only at very low frequencies (i.e., at small potential scan rates). Whereas at higher frequencies,

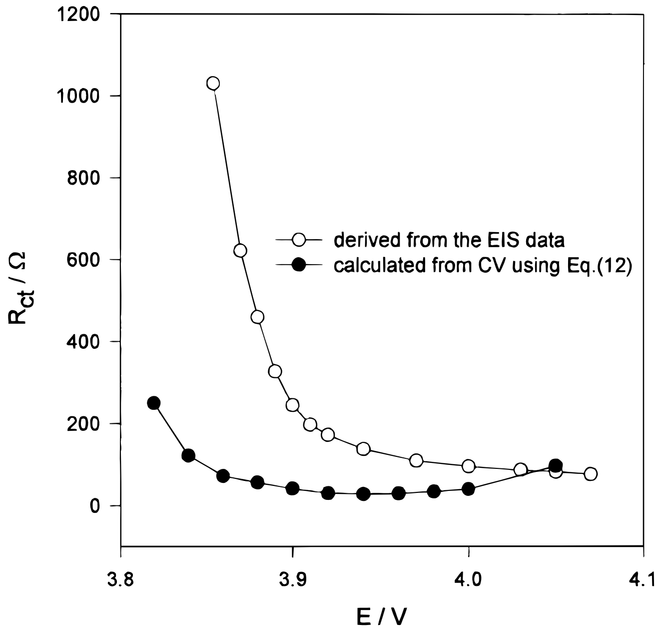

Figure 5. Plot of the charge-transfer resistance vs. potential. (——) Theoretical curve calculated using Eq. 12 with $Q_t = 0.28$ C, $\nu = 10$ μV/s, and $K = 40$ (note that $k_o = K/\delta f \nu$). The transfer from x to $(E - E_o)$ was performed with use of Eq. 5. (○) The R_{ct} vs. E plot obtained by fitting the experimental Nyquist plots with the Voigt and FMG impedance model.

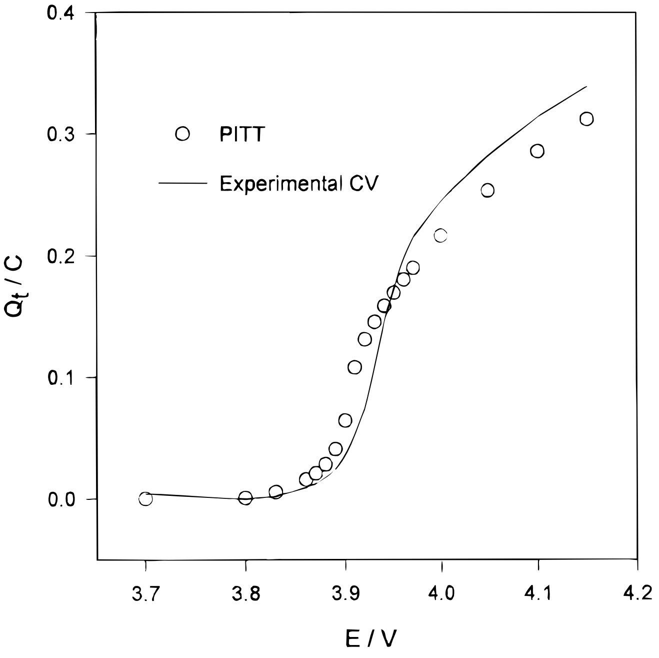

Figure 7. Plots of the charge vs. potential during the deintercalation obtained by integration of the experimental CV curve (solid line, $\nu = 10$ μV/s) and the incremental ΔQ vs. E curve measured by the potentiostatic intermittent titration (○).

S0013-4651(98)05-018-6 CCC: $7.00 © The Electrochemical Society, Inc.

the resolution of EIS and PITT is sharper with respect to the relevant relaxation processes. This is observed in the low-to-medium frequency domain, wherein solid-state diffusion of Li ions is the rate-determining step of the intercalation process. The application of EIS and PITT results in highly correlated values of diffusion time, τ, vs. E (Fig. 4a), whereas only a single averaged value of τ (and thus of D) can be obtained from SSCV using Eq. 11 ($\tau = 275$). This is about 40 times less than the peak value obtained from EIS and PITT. In the case of solution redox species, all three techniques should provide the same kinetic information.

The values of D obtained in this work (Fig. 4b), which vary from $\log D = -10$ to $\log D = -11.6$ (here and below, D is expressed in cm^2/s), are much closer to those values reported for thin $Li_{1-x}CoO_2$ films than those reported for powder electrodes. According to Ref. 39, $Li_{1-x}CoO_2$ thin films are characterized by $\log D = -10$ obtained from GITT experiments. Barker et al.[2] also reported a nonmonotonic D vs. x plot for their $Li_{1-x}CoO_2$ electrode, very similar to ours. However, the absolute values of D obtained by these researchers were about one order of magnitude larger than ours, which certainly can be attributed to different assumptions for the values of l. Nonmonotonic shapes of D vs. x plots have also been observed for a number of other intercalation materials. Barker et al.[42] presented D vs. x data of high resolution for $Li_{1-x}Mn_2O_4$ spinel electrodes. Using GITT, they obtained D vs. x plots with two minima, corresponding to the two peaks in the SSCV, which relate to the redox transfers between the cubic spinel phases.

For the porous $Li_{1-x}CoO_2$ electrode, $\log D$ was found to be confined between -8.7 and -7.4.[40] Once again, we ascribe this difference to uncertainty in the determination of l. Sometimes the effective diffusion length, l, is identified with the thickness of the powder electrode, which may result (for thick electrodes) in unjustified large values of D. Although a narrow differential capacity peak is observed,[41] the reported independence of D on x for Li-ion insertion electrodes relates to resolution problems (as explained previously). We suggest that the nonmonotonic variation of $\log D$ with x showing a minimum in the vicinity of the peak potential on the differential capacity curve results from attractive short-range interactions between the intercalation sites. Very strong attractive interactions ($g < -4$) which lead to phases separation in the electrode bulk imply that in the potential domain of the phase separation, the chemical diffusion coefficient reflects an effective value which includes the contribution from diffusion in both phases (see also the following sections).

The text below describes the characteristics of kinetic charge-transfer limitations of these electrodes. EIS provides well-resolved data from which the dependence of R_{ct} on the potential and the intercalation level is clearly elucidated (provided that our assignment for the medium-frequency semicircle in the impedance spectra is correct). We observe a decrease in the R_{ct} as the potential increases. We find some correlation between the drop of R_{ct} at the high-potential region and a drastic (two orders of magnitude) increase of the electronic conductivity of this material (obtained by in situ conductivity measurements[43]). The conductivity of $Li_{1-x}CoO_2$ during Li-ion extraction was increased exponentially with potential in the range from 3.0 to 3.9 V. We note the lack of complete overlapping (in potentials) between the decrease in the medium frequency semicircle observed in our EIS measurements and the increase in the active mass conductivity measured around 4 V. Thus, we assume that the variations of R_{ct} vs. E measured by EIS reflect not only the transition of $Li_{1-x}CoO_2$ from the semiconducting to the conducting domain, but rather may be connected with some other aspects.

The influence of the slow interfacial kinetics on the cyclic voltammetric response (the parameter $K = k_o/\delta f \nu$, Eq. 2) is studied by the analysis of the SSCV peak profile and the peak-potential separation, which may depend on side effects, such as uncompensated ohmic potential drops and slow Li-ion migration. Consequently, we can conclude that the R_{ct} values measured by EIS are certainly more resolved and meaningful than those obtained from the SSCV (Eq. 12 and Fig. 5). The internal ohmic potential drops in these composite electrodes that interfere with the intrinsic kinetics of the Li insertion process into the active mass can be almost eliminated when the electrodes are thin and contain sufficient conductive additives. The thinner the electrode and the slower the scan rate (increasing K, see Fig. 2c), the better their intrinsic kinetics and thermodynamics are reflected by the SSCV (accumulation of Li via a first-order phase transfer) beyond diffusion control.

Comments on the nature of the phase transition in $Li_{1-x}CoO_2$.—Figure 8 shows schematically the behavior of the Frumkin-type insertion/deinsertion isotherm at $g > g_{crit}$ and $g < g_{crit}$ ($g_{crit} = -4$). At $g < g_{crit}$, the isotherm is S-shaped; as the system approaches the points denoted as x_1 and x_2 in Fig. 8, a phase transition occurs along the vertical lines h_1 and h_2. Hence, intercalation and deintercalation occur with an intrinsic hysteresis (peak separation Eh_1 - Eh_2). This also appears at equilibrium in the absence of any kinetic or diffusion barriers ($k \rightarrow \infty$ in Eq. 2).[28] Hence, at $g = -4$ (Eq. 1, 2), there should be no intrinsic hysteresis. At g = -4.2, which has been found for the $Li_{1-x}CoO_2$, the predicted intrinsic hysteresis is minute (in the order of a few milivolts).

The evaluated potential width for the intrinsic hysteresis is the *minimal* and corresponds to a completely *quasi-equilibrium* phase transition. However, conventional relaxation processes, such as slow interfacial kinetics (small K) and solid-state diffusion, may considerably increase the hysteresis width. This is evident from the experimental curves in Fig. 2a and b, the simulated ones in Fig. 2c, and is schematically shown in Fig. 8. The intrinsic hysteresis of the $Li_{1-x}CoO_2$ electrodes at quasi-equilibrium conditions is also evident from EIS. Nyquist plots of the $Li_{1-x}CoO_2$ electrode measured at the same potentials during insertion and deinsertion of Li ions also show hysteresis of these plots in the low-frequency domain (not presented here). This hysteresis appears as differences in the Z'' values obtained during intercalation and deintercalation at the lowest frequency applied (5 mHz), and hysteresis corresponds nicely to that observed in the SSCV curves.

The nature of such a quasi-equilibrium hysteresis appearing in charging curves of insertion processes has been theoretically discussed by Vorotyntsev and Badiali.[28] Their calculations show that

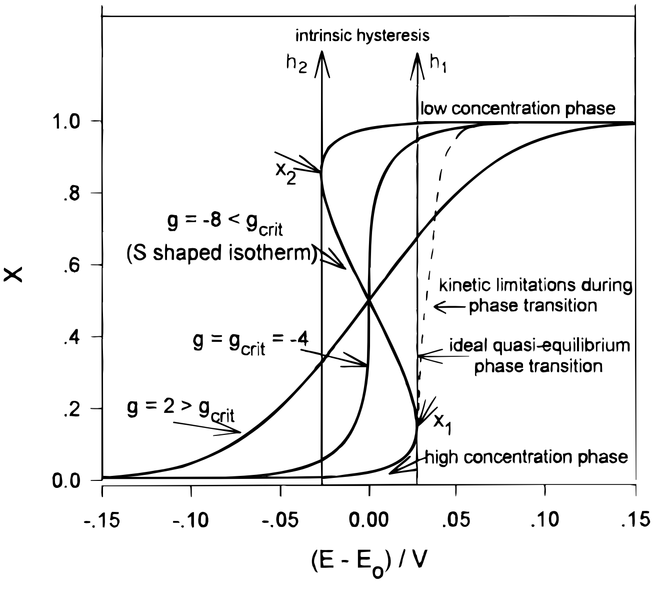

Figure 8. Charge-discharge curves calculated according to the Frumkin-type insertion isotherm (Eq. 1) showing a first-order phase transition at $g < g_{crit}$ (dashed vertical lines at the inflection points x_1 and x_2 during charging and discharging, respectively).The correponding S-shaped isotherm possesses an intrinsic hysteresis resulting in the SSCV peak separation at the quasi-equilibrium charge-discharge conditions. The gradually increasing solid curve starting at the right inflection point schematically situation depicts the under a kinetic control. The ideal phase transition occurs at $g = -4$. Continuous charging is demonstrated for $g = 2$.

S0013-4651(98)05-018-6 CCC: $7.00 © The Electrochemical Society, Inc.

the intrinsic voltammetric behavior of such systems may lead to narrow SSCV peaks (about 5-10 mV), based on the rough theoretical estimation. This may extend the range of potentials in which the phase transition takes place (see Fig. 8) instead of infinitely high peaks expected for ideal phase transfer processes.

Alternatively, we can explain the narrow peaks on SSCV curves and their intrinsic hysteresis during the insertion-deinsertion process by the so-called droplet formation mechanism. According to this explanation, a new phase is formed in the bulk of the old one as small islands.[28] From theoretical simulations of the SSCV curves for this particular relaxation mechanism, one should expect the appearance of narrow peaks of specifically symmetric shape which are proportional to the scan rate and exhibit only slight change in peak potential with the scan rate (compare with the features of the plots in Fig. 2a and c discussed above).

Li-ion insertion/deinsertion into/from $Li_{1-x}CoO_2$ occurs as a transition between two crystallographically different phases, as evidenced from the in situ XRD data.[1,12] An important question is to what extent is a Frumkin-type isotherm valid for modeling transition between two phases without distinct specification of their molecular (atomic) arrangements. Based on Ref. 44, in which the case of random site distribution is compared with cases of particular molecular arrangements, we assume that ignoring such molecular arrangements cannot radically change the picture of the phase transition described in terms of the Frumkin isotherm, as such an isotherm generally accounts for intersite interactions.

It is also important to discuss to what extent the picture of the transition between the low- and high-density phases (at $g < g_{crit}$, see Fig. 8) corresponds to the available in situ XRD data for the $Li_{1-x}CoO_2$.[1,12] Indeed, the latter studies clearly show that when charging is performed at a slow scan rate, the range of potentials for the two-phase coexistence is narrow and comparable with the half-peak width of the differential capacity curves. This means that the same relaxation processes that control the potential variations of the differential capacity determine the ratio between the coexisting phases.

Examining these reported in situ XRD experiments,[1,12] we exclude a possible nonequilibrium situation in the electrode in which, under a driving force such as a potential step, the small particles are fully converted to the high-Li-density phase, whereas in the larger particles, there is a delay in conversion. Under pure quasi-equilibrium conditions, at the end of a potential step we expect to obtain two coexisting phases at each $Li_{1-x}CoO_2$ particle, with relative distinct boundaries between them. Hence, the question arises to what extent the semi-infinite diffusion model is valid for situations when the intercalation proceeds partially via a movement of the interphase boundaries.

This important issue was discussed by McKinnon and Haering.[18] They showed theoretically that the application of a constant current method for the determination of D (in case of the three most important geometries of the diffusion flux: linear one-dimensional, cylindrical, and spherical) results in different analytical expressions for D. They examined two alternative charging possibilities: continuous (solid-solution formation) and noncontinuous (via a moving boundary). The latter model clearly relates to the first-order phase transition. Except for one-dimensional diffusion within the range of relatively small current densities, it was impossible to distinguish between these two alternative diffusion mechanisms. Another example of a "diffusion-like" behavior during propagation of moving boundaries can be observed during insulator-to-metal transitions in conducting polymers (the so-called memory effect).[45] In any case, these considerations justify the term "effective" chemical diffusion coefficient applied to two-phase coexistence regions.[2].

The Frumkin isotherm, chemical diffusion coefficient, and the enhancement factor.—Treating the thermodynamic and mass-transport properties of some solid ion-conductors, Weppner and Huggins[35] proposed an expression which connects the chemical and self-diffusion coefficients of the related ionic species, D and D_o

$$D = D_o L = D_o \, d \ln a_{Li^+}/d \ln c_{Li^+} \qquad [14]$$

with the enhancement factor L

$$L = d \ln a_{Li^+}/d \ln c_{Li^+} = (e/kT)x(dE/dx) \qquad [15]$$

where k is the Boltzmann constant and e is the electron charge.

Hence, the enhancement factor is the contribution to D due to interaction between the diffusing species and the medium, depending on their concentration. The chemical diffusion coefficient is also connected with the mobility, M, of the diffusing species according to the Einstein formula

$$D_o = MkT \qquad [16]$$

Equation 14 describes activities of the diffusing species, and thus can be used for analyzing particular cases. McKinnon and Haering[18] were the first to address the issue of deriving the enhancement factor for insertion processes described by Langmuirian and Frumkin-type isotherms. In general, the chemical diffusion coefficient is defined as follows

$$D = (a^2k^*)(1 - x)x(\partial\mu_{Li^+}/\partial x)(kT)^{-1} \qquad [17]$$

The separate terms of Eq. 17 are ascertained with the following important diffusion characteristics. $M_o = a^2k^*/kT$ expresses ionic mobility of a pure phase ($x = 1$) in terms of a hopping rate constant k^* and a nearest neighbor separation a. For a one-dimensional lattice model, we assume that at $x \neq 1$, the value of M decreases because of the occupation of the neighboring sites: $M = M_o(1 - x)$. Thus, combining Eq. 14, 16, and 17 we obtain

$$L = x(\partial\mu_{Li^+}/\partial x)(kT)^{-1} \qquad [18]$$

which is a general definition of the enhancement factor that may be applied to any lattice model.

The Frumkin isotherm implies the following equation for the chemical potential of Li ions in the solid matrix

$$\mu_{Li^+} = \mu^0_{Li^+} + kT \ln x/(1 - x) + kTgx \qquad [19]$$

Equation 19 takes into account the availability of sites only for a single kind of species, Li ions, whereas the counterbalancing electronic species are treated as noninteracting (ideal gas approximation). The dominance of ionic species in determining the availability of sites is justified because the shape of the plot of the dc electronic conductivity of $Li_{1-x}CoO_2$ vs. electrode potential does not correspond to the potential variations of its differential capacity (the former plot as opposed to the latter one is not a peak-shaped function[43]). This finding contradicts conventional redox polymers,[27] where redox capacity correlates with the electronic conductivity rather than with ionic conductivity. Thus, their redox capacity depends primarily on the availability of localized electronic sites.[27]

By a combination of Eq. 18 and 19, one can derive an expression for the enhancement factor corresponding to the Frumkin isotherm

$$L = (1 - x)^{-1}[1 + g(1 - x)x] \qquad [20]$$

Hence, for the chemical diffusion coefficient normalized by M_o, D takes the following form

$$(\text{normalized } D) = D/(a^2k^*) = 1 + g(1 - x)x \qquad [21]$$

For insertion processes to which a Frumkin-type isotherm can be applied, Eq. 19-21 are very useful for characterizing cases in which $g > g_{crit} = -4$. For the Langmuirian isotherm $g = 0$, D is therefore independent of x.

At $g > g_{crit}$ D vs. x has a minimum at $x = 0.5$ (see Eq. 21), always retaining positive values. At the critical value $g = -4$, both L and D reach zero value, whereas at $g < g_{crit}$ (nonmonotonous charging due to the phase transition), L and D assume negative values along the unstable S-shaped part of the isotherm (Fig. 8).

Equations 15-21 describe an insertion process in which $0 < x < 1$. In this paper, we concentrate on the intercalation of Li into $Li_{1-x}CoO_2$ where $0.75 < 1 - x < 1$ ($0 < x < 0.25$). However, these equations are easily applicable to the present case, taking $Li_{0.75}CoO_2$ as the fully deintercalated phase (corresponding to $x = 0$ in Eq. 15-21). Equation 21 clearly demonstrates the following: when we have insertion with strong attractive interactions and first-order phase transition involving intrinsic hysteresis between the insertion and deinsertion processes, *D*, the effective diffusion coefficient calculated, is not defined at the intercalation levels (and the potential) along the unstable branch of the intercalation isotherm (i.e., in the vicinity of $x = 0.5$ in Eq. 21).

In fact, the experimental results accurately reflect these situations, as *D* vs. *E* and *x* plots have sharp minima around the C_{int} peak potential. Practically, at this minima, *D* has a certain positive value, because even at the lowest scan rates (SSCV) or the smallest potential steps (PITT) applied, we lack equilibrium or quasi-equilibrium conditions, and the electrode response measured is kinetically controlled. Our model, which both assumes attractive interactions between the intercalation sites and can be described by a Frumkin isotherm (complicated by Butler-Volmer kinetic limitations), is too simplified for the complicated, multistep Li insertion into the composite electrode. Nevertheless, this relatively simple model predicts several key features of these systems: intrinsic hysteresis between insertion and deinsertion, the shape of the C_{int} vs. *x*, *E* curves, and the nonmonotonic, peak-shaped behavior of *D* vs. *x*, *E*.

D vs. *E* curves measured during insertion and deinsertion of Li into $\text{Li}_{1\text{-}x}\text{CoO}_2$ show a similar hysteresis as the SSCV curves (the minima in *D* vs. *E* coincide with the maxima of C_{int} vs. *E*). The hysteresis obtained in *D* vs. *E*, measured during Li insertion and deinsertion, can be semiquantitatively, theoretically predicted by a combination of Eq. 2 and 21 for different magnitudes of the kinetic limitations (expressed by $K = k_o/\delta f \nu$ in Eq. 2). *x* vs. *E* values during intercalation and deintercalation can be calculated for different values of *K* by numerical integration of Eq. 2 using incremental potential step (1 mV). $\int IdE$ corresponds directly to *x*, and thereby, its integration provides the dependence of *x* vs. *E* for different scan rates. These values are incorporated in Eq. 21.

Figure 9 illustrates the resulting theoretical log *D* vs. *E* plots for three different values of *K*, for both insertion and deinsertion processes. We conclude the following from this figure

1. Quasi-equilibrium log *D* vs. *E* curves exhibit a discontinuity region close to the SSCV peaks (where $L < 0$). Their width increases (7, 14, and 21 mV as the kinetic limitations are more pronounced, corresponding to values of 80, 16, and 1.6 for *K*).

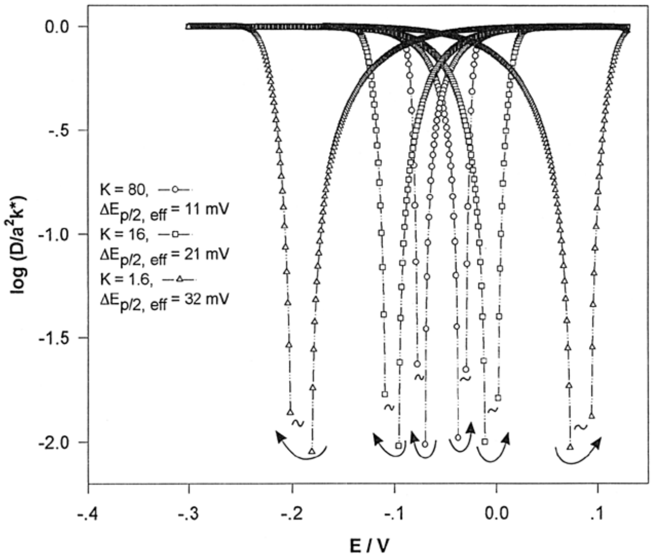

Figure 9. Plots of log D/a^2k^* vs *E* calculated with the use of Eq. 21 and 2. The values of the dimensionless kinetic constants are shown. The attraction constant in all three cases is $g = -4.2$. Numerical integration of the simulated SSCV curves was performed to obtain $x = x(E - E_o)$ dependencies required for the calculation of *D* (Eq. 5). Arrows indicate the direction of the potential scans.

2. Once PITT is performed at potential steps larger than the width of the discontinuity region, the results obtained may be unresolved and meaningless.

3. The amplitude of log *D* variation with the potential for all three values of *K* calculated in Fig. 9 approximates two orders of magnitude (for 1 mV potential increments). This compares with the amplitude of log D vs. E observed experimentally for the $\text{Li}_{1-x}\text{CoO}_2$ (c/f Fig. 9 and 4b). However, the experimental plots are much broader than the theoretical ones (~60 mV vs. 10-20 mV). This may be partially connected with the internal ohmic potential drops and the slow Li^+ migration through the surface films, both overlapping with the Cottrell region of the $It^{1/2}$ vs. log *t* curves from which *D* is calculated. Another reason for broadening of the experimental values may be the higher values of the practical R_{ct} compared with the theoretical ones (Eq. 12), especially in the potential range between 3.8 and 4.0 V (see Fig. 5).

4. Our relatively simple model predicts the hysteresis in log *D* vs. *E* plots which increases as the perturbation due to slow kinetics increases and is similar to the corresponding hysteresis in the SSCV (cf. Fig. 9 and 2), as was found experimentally.

5. The minima in log *D* vs. *E* generally reflect the presence of strong attractive interactions between the intercalation species. When $-4 < g < 0$, and hence $L > 0$ and $D > 0$, the Frumkin isotherm predicts a uniform (continuous) charging (*Q* vs. *E*, *x*) of the material. When $g < -4$, there is a narrow potential domain in which both *L* and the theoretical $D < 0$, the charging curves, consist of two domains: the first one is linked to the potentials corresponding to the foot of the SSCV (uniform charging), whereas the second one refers to a narrow region of potentials in which a first-order phase transition occurs. Meaningless, negative theoretical values of *D* in this model correspond to the unstable S-shaped branch of the intercalation isotherm. The experimentally calculated *D* values at this narrow potential domain reflect the kinetically controlled, first-order phase transition, as shown schematically in Fig. 8.

Conclusion

Li-ion deinsertion from thin $\text{Li}_{1-x}\text{CoO}_2$ electrodes has been studied using simultaneous application of SSCV, PITT, and EIS. The experimental cyclic voltammetric curves were fitted using an equation obtained by a combination of the Frumkin-type sorption isotherm with the Butler-Volmer kinetic equation for the slow Li-ion interfacial charge transfer. The apparent attraction constant was found to be -4.2, which is characteristic of a quasi-equilibrium, first-order phase transition.

In this study, all three electroanalytical techniques used resulted in similar semiquantitative dependence of the differential intercalation capacity and the characteristic diffusion time on the electrode potential (and the intercalation level). This correlation can only be obtained when a finite space situation exists in thin electrodes.

The effective chemical diffusion coefficient was found to be a peak-shaped function of the electrode's potential with a minimum at the potential in which the intercalation capacity vs. potential is maximal. This behavior is also predicted by an intercalation model described by the Frumkin-type insertion isotherm. The depth of the log *D* vs. *E* plots (i.e., their resolution) depends on the height of potential steps used.

The enhancement factor of the effective chemical diffusion coefficient has been analyzed within the framework of the Frumkin sorption isotherm.

The impedance spectra of these electrodes reflect the serial character of the overall insertion process of Li into $\text{Li}_{1-x}\text{CoO}_2$. This includes several steps in series (e.g., Li^+ migration through surface films, charge transfer, solid-state diffusion, accumulation, etc.). The EIS demonstrates a separation of the various time constants of these processes. This led us to suggest the equivalent circuit analog based on a Voigt-type analog in series with the FMG impedance (finite-length Warburg-type element in series with capacitance). As was already shown, this model is appropriate for describing intercalation processes in highly oriented materials. Despite the excellent fit obtained between

S0013-4651(98)05-018-6 CCC: $7.00

simulated impedance spectra and experimental ones, clearly this is not the only model that explains the behavior of these electrodes.

Acknowledgments

This study was partially supported by the BMBF, the German Ministry of Science, and the Israeli Ministry of Science and Technology. We are deeply grateful to Dr. L. Daikhin and Dr. Y. Gofer for their stimulating discussions and valuable comments.

Bar-Ilan University assisted in meeting the publication costs of this article.

References

1. J. N. Reimers and J. R. Dahn, *J. Electrochem. Soc.*, **139**, 2091 (1992).
2. J. Barker, R. Pynenburg, R. Koksbang, and M. Y. Saidi, *Electrochim. Acta*, **41**, 2481 (1996).
3. M. G. S. R. Thomas, P. G. Bruce, and J. B. Goodenough, *J. Electrochem. Soc*., **132**, 1521 (1985).
4. T. Ohzuku and A. Ueda, *J. Electrochem. Soc*., **144**, 2780 (1997).
5. G. Pistoia, A. Antonini, R. Rosati, and D. Zane, *Electrochimica Acta*, **41**, 2683 (1996).
6. T. Ohzuku, A. Ueda, M. Nagayama, Y. Iwakoshi, and H. Komori, *Electrochim. Acta*, **38**, 1159 (1993).
7. E. Plichta, S. Slane, M. Uchiyama, M. Salomon, D. Chua, W. B. Ebner, and H. W. Lin, *J. Electrochem. Soc.*, **136**, 1865 (1989).
8. B. Garcia, J. Farcy, J. P. Pereira-Ramos, J. Perichon, and N. Baffier, *J. Power Sources*, **54**, 373 (1995).
9. C. Y. Yao, T. H. Kao, C. H. Cheng, J. M. Chen, and W.-M. Hurng, *J. Power Sources*, **54**, 491 (1995).
10. S. Yamada, M. Fujiwara, and M. Kanda, *J. Power Sources*, **54**, 209 (1995).
11. R. Yazami, N. Lebrun, M. Bonneau, and M. Molteni, *J. Power Sources*, **54**, 389 (1995).
12. T. Ohzuku and A. Ueda, *J. Electrochem. Soc.*, **141**, 2972 (1994).
13. R. B. Goldner, Te-Yang Liu, and S. Slaven, *J. Electrochem. Soc.*, **143**, L129 (1996).
14. M. D. Levi and D. Aurbach, *J. Phys. Chem. B*, **101**, 4630 (1997).
15. M. D. Levi and D. Aurbach, *J. Phys. Chem. B*, **101**, 4641 (1997).
16. M. D. Levi and D. Aurbach. *J. Electroanal. Chem*., **421**, 79 (1997).
17. D. Aurbach, M. D. Levi, E. Levi, and A. Schechter, *J. Phys. Chem. B*, **101**, 2195 (1997).
18. W. R. McKinnon and R. R. Haering, in *Modern Aspects in Electrochemistry*, Vol. 15, p. 235, Plenum Press, New York (1987).
19. D. Aurbach, M. D. Levi, E. Levi, G. Salitra, B. Markovsky, and H. Teller, *J. Electrochem. Soc*., **145**, 3024 (1998).
20. D. Aurbach, *J. Electrochem. Soc.*, **136**, 906, 1606, 1611 (1989).
21. D. Aurbach and H. E. Gottlieb, *Electrochim. Acta*, **34**, 141 (1989).
22. E. Laviron, *J. Electroanal. Chem*., **52**, 395 (1974).
23. E. Gileadi and B. E. Conway, in *Modern Aspects of Electrochemistry*, J. O'M. Bockris and B. E. Conway, Editors, Vol. 3, p. 347, Butterworths, London (1964).
24. A. P. Brown and F. C. Anson, *Anal. Chem.*, **49**, 1589 (1997).
25. B. E. Conway, *Electrochim. Acta.*, **38**, 1249 (1993).
26. M. . Mathias and O. Haas, *J. Phys. Chem.*, **96**, 3174 (1992).
27. C. E. D. Chidsey and R. W. Murray, *J. Phys. Chem.*, **90**, 1479 (1986).
28. M. A. Vorotyntsev and J. P. Badiali, *Electrochim. Acta.*, **39**, 289 (1994).
29. H. Angerstein-Kozlowska, J. Kleinger, and B. E. Conway, *J. Electroanal. Chem*., **75**, 45 (1977).
30. J. O.'M Bockris and S. U. H. Khan, *Surface Electrochemistry, A Molecular Level Approach*, Chap. 3, p. 224, Plenum Press, New York, London (1993).
31. G. Inzelt, in *Electroanalytical Chemistry*, A. J. Bard, Editor, Vol. 18, p. 89, Marcel Dekker, New York, (1994).
32. K. Aoki, K. Tokuda, and H. Matsuda, *J. Electroanal. Chem.*, **146**, 417 (1983).
33. J. R. Dahn and R. R. Haering, *Solid State Ionics*, **2**, 19 (1981).
34. C. J. Wen, B. A. Boukamp, R. A. Huggins, and W. Weppner, *J. Electrochem. Soc.*, **126**, 2258 (1979).
35. W. Weppner and R. A. Huggins, *Ann. Rev. Mater. Sci.*, **8**, 269 (1978).
36. C. Ho, I. D. Raistrick, and R. A. Huggins, *J. Electrochem. Soc.*, **127**, 343 (1980).
37. A. J. Bard and L. R. Faulkner, *Electrochemical Methods*, p. 101, John Wiley & Sons, Inc., New York (1980).
38. J. R. MacDonald, *Impedance Spectroscopy*, p. 60, Wiley, New York (1987).
39. K. A. Strievel, C. Z. Deng, S. J. Wen, and E. J. Cairns, *J. Electrochem. Soc.*, **143**, 1821 (1996).
40. A. Honders, J. M. der Kindern, A. H. van Heeren, J. H. W. de Witt, and G. H. J. Broers, *Solid State Ionics*, **15**, 265 (1985).
41. D. Guyomard and J. M. Tarascon, *J. Electrochem. Soc*., **139**, 937 (1992).
42. J. Barker, R. Pynenburg, and R. Koksbang, *J. Power Sources*, **52**, 185 (1994).
43. M. Shibuya, T. Nishina, T. Matsue, and I. Ichida, *J. Electrochem. Soc.*, **146**, 3157 (1996).
44. M. Matsuda, K. Aoki, and K. Tokuda, *J. Electroanal. Chem.*, **217**, 1, 15 (1987).
45. M. A. Vorotyntsev, Abstract 1275, p. 1449, The Electrochemical Society and the International Society of Electrochemistry Meeting Abstracts, Vol. 97-2, Paris, France, Aug 31-Sept 5, 1997.